Electronic Transactions on Numerical Analysis.
Volume 30, pp. 258-277, 2008.

ISSN 1068-9613.

ETNA
Kent State University
http://etna.math.kent.edu

OPTIMAL DISCRETIZATION OF PML FOR ELASTICITY PROBLEMS*

VADIM LISITSA†

Abstract. This paper presents a generalization of the optimal finite-difference perfectly matched layer (PML) approach to isotropic elasticity. It allows the use of methods of rational approximation theory for a clever choice of discretization parameters in order to essentially reduce reflection coefficients for a wide range of incident angles while using a small number of grid points.

Key words. artificial boundary conditions, optimal grids, perfectly matched layers, finite-difference schemes, rational approximation

AMS subject classifications. 65N06, 74C02

1. Introduction.

Numerical modeling of seismic wave propagation is a very important tool providing unique possibilities in such areas as survey design for complicated media, finite-difference reverse-time migration, and so on. The key constituent of any efficient implementation of finite-difference simulation is a procedure which makes possible the performance of computations within some bounded spatial domain (target area) and avoids any significant artificial reflections.

There are two main approaches to provide this:

- Absorbing boundary conditions (ABCs) which were first proposed and developed in [6]. These conditions are based on rational approximation of a square root which appears when one writes down exact transparent conditions in a phase space.
- Perfectly matched layer (PML) presented in the paper [2]. Under this approach, one should introduce some special layer surrounding the target area. The interface between this layer and the target area does not provide any significant reflections while the layer itself attenuates waves. The discrete model of the PML can contain up to 50 points in width and sometimes is rather time-consuming in its finite-difference implementation; computations inside the PML can demand up to a quarter of the total computational time.

There are a variety of alternative ways to provide efficient truncation of a target area with low reflecting artificial boundary conditions. One of them, e.g., is based on exact boundary conditions proposed in [8]. The other one is optimal PML. This method for the scalar wave equation was proposed in [1] and is a combination of ideas presented in [5, 7]. The differential model of this method was obtained by a particular change of variables, which is actually a special case of the standard PML. Implementation of the optimal grids [4] permits a reduction of the number of points in the discrete model of the optimal PML. In this paper, we present the expansion of this approach to isotropic elasticity problems and provide numerical experiments illustrating the efficiency of the approach. Throughout the paper, we will refer to the original approach for the scalar wave equation presented in [4] and call it, for simplicity, "the scalar problem".

The paper has the following structure. In Section 1.1, we describe the artificial boundary conditions in more detail and explain the main ideas of the optimal PML for the wave equation. Section 2 contains the construction of the optimal PML for elasticity problems. A

*Received September 4, 2006. Accepted for publication November 26, 2007. Published online on October 16, 2008. Recommended by V. Druskin. This work was done in cooperation with Schlumberger Moscow Research and partially supported by RFBR grants # 05-05-64227, 06-05-64748, 07-05-00538, and 08-05-00265.

†Institute of Petroleum Geology and Geophysics, Siberian Branch of the Russian Academy of Science, 630090 Novosibirsk, Russia (lisitsavv@ipgg.nsc.ru).

ETNA
Kent State University
http://etna.math.kent.edu

finite-difference scheme in physical space for PML is presented and studied in Section 3. The numerical experiments are described and discussed in Section 4.

1.1. Artificial boundary conditions for wave equation. Let us consider the 2D wave equation,

$$\hat{u}_{tt} - \hat{u}_{xx} - \hat{u}_{yy} = 0,$$

in the domain, $t > 0,\ x < 0,\ y \in \mathbb{R}$. Suppose that a "reflectionless" boundary condition is to be constructed on the boundary $x = 0$. We also assume that a source is placed deep enough inside the regular domain, so that only the propagative modes can be considered on the boundary. Artificial boundary conditions are constructed in the spectral domain, so we need to implement the Fourier transform,

$$u(\omega, x, \eta) = \int_{-\infty}^{\infty}\int_{-\infty}^{\infty} \hat{u}(t, x, y) e^{i(\omega t + \eta y)}\, dt\, dy, \tag{1.1}$$

and obtain the equation,

$$u_{xx} + i\omega\left(1 - \theta^2\right)u = 0, \tag{1.2}$$

where $\theta = \frac{\eta}{\omega}$. We will also need another form of this equation,

$$u_{xx} + i\omega\Lambda u = 0,$$

where $\Lambda = 1 - \theta^2$. As soon as only propagative modes are considered, $\Lambda \in [0, 1]$.

Let us now describe the ABC's construction. The equation (1.2) possesses two plane wave solutions. The first one propagates to the right, while the second moves to the left. Therefore, the natural way to avoid reflections from the boundary $x = 0$ is to cancel the second mode on the boundary. This leads to the condition,

$$u = \frac{-1}{i\omega\sqrt{\Lambda}} u_x|_{x=0}. \tag{1.3}$$

In order to implement this condition in physical space, the inverse Fourier transform should be performed. However, this results in a nonlocal operator. Use of this operator for finite-difference simulation is complicated and computationally expensive. The main idea of ABC [6] is to construct a rational approximation of the square root, so that the condition (1.3) transforms to

$$u = -\frac{P^{n-1}(\Lambda)}{i\omega P^n(\Lambda)} u_x|_{x=0},$$

where $P^n(\Lambda)$ is a polynomial of degree n. The inverse Fourier transform of the rational function can be easily obtained using the pole-residues theorem and provides one with local boundary conditions. This approach is low cost and efficient. Nevertheless, it has two disadvantages. ABC is quite difficult for implementation at the corners of the target area and becomes complicated for elasticity problems where more than one propagative mode exists.

The second type of reflectionless condition considered in the paper is PML. Assume the equation (1.2) is stated for $x < 0$. Following [2], one can introduce an artificial layer for $x > 0$ and implement the complex change of variables inside the layer,

$$\frac{d}{dx} = \left(\alpha + \frac{\beta}{i\omega}\right)\frac{d}{d\tilde{x}}. \tag{1.4}$$

ETNA
Kent State University
http://etna.math.kent.edu

This change of variables transforms propagative modes to evanescent ones if $\beta \neq 0$. The PML is simpler for implementation than ABC, but sometimes it needs as much as 50 points in x direction, which makes it computationally expansive.

Let us consider the optimal PML proposed in [1]. On the one hand, the Neumann-to-Dirichlet (NtD) problem can be stated for standard PML. That is, one must find a solution $u(0,\omega,\eta)$ of the problem,

$$\left(\alpha+\frac{\beta}{i\omega}\right)^{-1}\frac{d}{dx}\left(\left(\alpha+\frac{\beta}{i\omega}\right)^{-1}\frac{du}{dx}\right)+\omega^2\Lambda u=0,$$

$$\left(\alpha+\frac{\beta}{i\omega}\right)^{-1}\frac{du}{dx}\bigg|_{x=0}=-1,$$

$$u|_{x=\infty}=0.$$

The solution of the NtD problem can be represented as

$$u(0,\omega,\eta,\alpha,\beta)=f_{\alpha\beta}(\omega,\eta)u_x(0), \tag{1.5}$$

where $f_{\alpha\beta}(\omega,\eta)$ is an NtD map, or impedance function. On the other hand, one can consider the discrete problem on a grid. Assume u is defined at points x_i, and u_x is assigned to points $\hat{x}_i$, on a grid. Defining the steps $h_i=x_{i-1}-x_i$ and $\hat{h}_i=\hat{x}_i-\hat{x}_{i-1}$, one can write down the finite-difference (f-d) NtD problem,

$$\left(\alpha+\frac{\beta}{i\omega}\right)^{-1}\hat{D}\left[\left(\alpha+\frac{\beta}{i\omega}\right)^{-1}Du_i\right]+\omega^2\Lambda u_i=0,$$

$$\left(\alpha+\frac{\beta}{i\omega}\right)^{-1}\hat{D}u_1=-1,$$

$$u_{k+1}=0,$$

where $Df_i=\frac{f_{i+1}-f_i}{h_i}$ and $\hat{D}=\frac{f_i-f_{i-1}}{\hat{h}_i}$. Solution u_1 of the f-d NtD problem can also be presented in terms of the NtD map,

$$u_1(\omega,\eta,\alpha,\beta)=f^k_{\alpha\beta}\left(\omega,\eta,h_i,\hat{h}_i\right)\hat{D}u_1. \tag{1.6}$$

The approximation error, in this case, is $\|u(0)-u_1\|\leq\|f_{\alpha\beta}-f^k_{\alpha\beta}\|\|u_x(0)\|=\delta^{\alpha\beta}\|u_x(0)\|$. So the discrepancy of the solution is defined by the error of the NtD map. As was proved in [1], the inequality,

$$\delta^{\alpha\beta}\geq\delta^{0\beta},$$

holds for any parameters α and β, where β is any real positive number. The f-d operator depends on the product of the grid steps and stretching factor β, so without loss of generality we assume that the latter is 1 and we vary the former to minimize the reflection. In this case, the NtD map of the differential problem becomes $f(\Lambda(\omega,\eta))=1/\sqrt{\Lambda}$. The finite-difference NtD map is the rational function coinciding with the one appearing in the description of ABC. The principal difference between optimal PML and ABC resides in the conversion of the rational function to the operator in the physical domain. The optimal PML allows one to represent the function in terms of spatial steps instead of high-order difference operators on the boundary as they appear for ABC. Below, we present the extension of this approach to elasticity problems.

ETNA
Kent State University
http://etna.math.kent.edu

2. Optimal PML for elasticity.

2.1. Statement of the problem.

First, let us recall the system of isotropic elasticity,

$$
\begin{aligned}
\rho\big(\hat{u}_x\big)_t &= \big(\hat{\sigma}_{xx}\big)_x + \big(\hat{\sigma}_{xy}\big)_y,\\
\rho\big(\hat{u}_y\big)_t &= \big(\hat{\sigma}_{xy}\big)_x + \big(\hat{\sigma}_{yy}\big)_y,\\
\big(\hat{\sigma}_{xx}\big)_t &= (\lambda+2\mu)\big(\hat{u}_x\big)_x + \lambda\big(\hat{u}_y\big)_y,\\
\big(\hat{\sigma}_{yy}\big)_t &= \lambda\big(\hat{u}_x\big)_x + (\lambda+2\mu)\big(\hat{u}_y\big)_y,\\
\big(\hat{\sigma}_{xy}\big)_t &= \mu\big(\hat{u}_y\big)_x + \mu\big(\hat{u}_x\big)_y,
\end{aligned}
\tag{2.1}
$$

where $\hat{u}_x$ and $\hat{u}_y$ are the components of the velocity vector. Functions $\hat{\sigma}_{xx}$, $\hat{\sigma}_{yy}$, and $\hat{\sigma}_{xy}$ are the components of the stress tensor. Parameter ρ is a density of the medium and $\lambda > 0$, $\mu > 0$ are the Lame parameters characterizing the medium properties. All the functions are defined inside the domain $t \geq 0,\ x \leq 0,\ y \in \mathbb{R}$. We will later use this particular representation of the system to write down the finite-difference scheme in a spatial domain. In order to construct the optimal PML, it is convenient to rewrite the system as

$$
\begin{aligned}
&\begin{bmatrix} 0 & A \\ A^* & 0 \end{bmatrix} \frac{\partial}{\partial x} \begin{bmatrix} \hat{w}_1 \\ \hat{w}_2 \end{bmatrix} + \begin{bmatrix} B_1 & 0 \\ 0 & B_2 \end{bmatrix} \frac{\partial}{\partial y} \begin{bmatrix} \hat{w}_1 \\ \hat{w}_2 \end{bmatrix}\\
&\qquad - \begin{bmatrix} C_1 & 0 \\ 0 & C_2 \end{bmatrix} \frac{\partial}{\partial t} \begin{bmatrix} \hat{w}_1 \\ \hat{w}_2 \end{bmatrix} = 0,
\end{aligned}
\tag{2.2}
$$

where the matrices are

$$
A = \begin{bmatrix} 1 & 0 \\ 0 & 1 \\ 0 & 0 \end{bmatrix}, \quad B_1 = \begin{bmatrix} 0 & 0 & 0 \\ 0 & 0 & 1 \\ 0 & 1 & 0 \end{bmatrix}, \quad B_2 = \begin{bmatrix} 0 & 1 \\ 1 & 0 \end{bmatrix},
$$

$$
C_1 = \begin{bmatrix} a_1 & 0 & a_3 \\ 0 & \rho & 0 \\ a_3 & 0 & a_1 \end{bmatrix}, \quad C_2 = \begin{bmatrix} \rho & 0 \\ 0 & a_2 \end{bmatrix},
$$

with

$$
a_1 = \frac{\lambda+2\mu}{4\mu(\lambda+\mu)}, \quad a_2 = \frac{1}{\mu}, \quad a_3 = \frac{-\lambda}{4\mu(\lambda+2\mu)},
$$

and vectors $\hat{w}_1 = (\hat{\sigma}_{xx}, \hat{u}_y, \hat{\sigma}_{yy})^T$, $\hat{w}_2 = (\hat{u}_x, \hat{\sigma}_{xy})^T$.

Following [1], assume the PML should be constructed in the x direction. Let us perform the Fourier transform (1.1) and pure imaginary change of variables for $x > 0$,

$$
\tilde{x} = \frac{1}{i\omega} x.
$$

This leads to the system of equations,

$$
i\omega \begin{bmatrix} 0 & A \\ A^* & 0 \end{bmatrix} \frac{d}{dx} \begin{bmatrix} w_1 \\ w_2 \end{bmatrix} + i\omega \begin{bmatrix} F_1 & 0 \\ 0 & F_2 \end{bmatrix} \begin{bmatrix} w_1 \\ w_2 \end{bmatrix} = 0,
\tag{2.3}
$$

where

$$
F_1 = \begin{bmatrix} -a_1 & 0 & -a_3 \\ 0 & -\rho & \theta \\ -a_3 & \theta & -a_1 \end{bmatrix}, \quad F_2 = \begin{bmatrix} -\rho & \theta \\ \theta & -a_2 \end{bmatrix},
$$

ETNA
Kent State University
http://etna.math.kent.edu

$\theta = \frac{\eta}{\omega}$. We also need to introduce additional spectral parameters, $\Lambda_p = \frac{1}{v_p^2} - \theta^2$, $\Lambda_s = \frac{1}{v_s^2} - \theta^2$.

Let us state the NtD problem for the PML. As one can see from (2.3), the variables are decoupled as two sets w_1 and w_2. It is convenient to consider the first set of variables as Dirichlet data and the second as Neumann data. Throughout this paper, we will consider w_1 as Neumann data and w_2 as Dirichlet data. The dual problem has no principal difference; therefore, we omit it. Consider the NtD problem

$$i\omega \begin{bmatrix} 0 & A \\ A^* & 0 \end{bmatrix} \frac{d}{dx} \begin{bmatrix} w_1 \\ w_2 \end{bmatrix} + i\omega \begin{bmatrix} F_1 & 0 \\ 0 & F_2 \end{bmatrix} \begin{bmatrix} w_1 \\ w_2 \end{bmatrix} = 0, \tag{2.4}$$

$$i\omega A^* w_1\big|_{x=0} = -i\omega w_1^0, \quad w_2\big|_{\tilde{x}=\infty} = 0,$$

where w_1^0 is assumed to be given Neumann data. The solution $w_2(0,\omega,\eta)$ should be found.

2.2. Construction of NtD map. The solution of the problem (2.4) can be represented as an action of the NtD map on Neumann data. In this section, the explicit form of the NtD map is constructed. In order to simplify the representation, let us rewrite the first boundary condition of (2.4) as

$$i\omega \begin{bmatrix} u_y \\ \sigma_{xx} \end{bmatrix}_{x=0} = -i\omega \begin{bmatrix} u^0 \\ \sigma^0 \end{bmatrix}.$$

Let us also recall the notation $w_2 = (u_x, \sigma_{xy})^T$.

THEOREM 2.1. *The solution of the problem (2.4) can be represented as*

$$\begin{bmatrix} u_x(0,\omega,\eta) \\ \sigma_{xy}(0,\omega,\eta) \end{bmatrix} = \left[R^s(\omega,\eta) f(\Lambda_s) + R^p(\omega,\eta) f(\Lambda_p)\right] \begin{bmatrix} u^0 \\ \sigma^0 \end{bmatrix},$$

where

$$f\left(\Lambda_j\right) = \frac{1}{\sqrt{\Lambda_j}}, \quad j = p, s,$$

are exact NtD maps corresponding to the scalar problem, for each scalar wave equation with velocities $v_{p,s}$. Matrices R^j have size 2×2 and are bounded functions of the parameters ω and η, so $\|R^j\| < \infty$.

Proof. Construction of the solution will be performed in the original terms of problem (2.4). In order to construct the solution of the problem, it is convenient to reformulate it in terms of generalized functions. Continue the functions for $x < 0$ and assume that w_2 is even and w_1 is odd. The jumps of $A^* w_1$ ought to be equal to $2w_1^0$. In this case, the problem becomes

$$\begin{bmatrix} 0 & A \\ A^* & 0 \end{bmatrix} \frac{d}{dx} \begin{bmatrix} w_1 \\ w_2 \end{bmatrix} + \begin{bmatrix} F_1 & 0 \\ 0 & F_2 \end{bmatrix} \begin{bmatrix} w_1 \\ w_2 \end{bmatrix} = \begin{bmatrix} 0 \\ -2w_1^0 \end{bmatrix}.$$

Implementing the Fourier transform,

$$\dot{f}(\xi) = \int_{-\infty}^{\infty} f(x) e^{i\xi x}\, dx,$$

one comes to the system of linear algebraic equations,

$$\begin{bmatrix} -a_1 & 0 & -a_3 & i\xi & 0 \\ 0 & -\rho & \theta & 0 & i\xi \\ -a_3 & \theta & -a_1 & 0 & 0 \\ i\xi & 0 & 0 & -\rho & \theta \\ 0 & i\xi & 0 & \theta & -a_2 \end{bmatrix} \begin{bmatrix} \dot{w}_1 \\ \dot{w}_2 \end{bmatrix} = \begin{bmatrix} 0 \\ -2w_1^0 \end{bmatrix}. \tag{2.5}$$

ETNA
Kent State University
http://etna.math.kent.edu

This system can be resolved analytically,

$$\dot{w}_1(0,\omega,\eta) = \left[R^s(\omega,\eta)\frac{-1}{\xi^2+\Lambda_s} + R^p(\omega,\eta)\frac{-1}{\xi^2+\Lambda_p}\right]w_1^0.$$

The exact representations of the matrices $R^j(\omega,\eta)$ are required neither for construction of the optimal discretization, nor for computation of the wavefield. Nevertheless, their boundedness should be proved. In order to do this, let us present the matrices

$$R^s = \begin{bmatrix} \dfrac{-v_s^{-2}+\Lambda_s}{\rho} & -\dfrac{3-v_p^2v_s^{-2}-2\Lambda_s v_s^2}{(v_p^2-v_s^2)}v_s^2\theta \\ -\dfrac{3-v_p^2v_s^{-2}-2\Lambda_s v_s^2}{(v_p^2-v_s^2)}v_s^2\theta & \dfrac{\mu(1+v_s^2\Lambda_s-v_s^4\Lambda_s^2)}{v_s^2} \end{bmatrix},$$

$$R^p = \begin{bmatrix} \dfrac{-\Lambda_p}{\rho} & -\dfrac{2\Lambda_s v_s^2-2v_s^2v_p^{-2}}{(v_p^2-v_s^2)}v_s^2\theta \\ -\dfrac{2\Lambda_s v_s^2-2v_s^2v_p^{-2}}{(v_p^2-v_s^2)}v_s^2\theta & \dfrac{\mu\theta(v_p^2-v_s^2-v_p^2v_s^2\Lambda_s)}{v_p^2} \end{bmatrix}, \tag{2.6}$$

where $\theta = \frac{\eta}{\omega}$ and $\Lambda_j = v_j^{-2} - \theta^2$. As soon as only propagative modes are considered, parameters $\Lambda_j \in [0, v_j^{-2}]$ and θ are bounded. Velocities of the P-wave $v_p = \sqrt{\frac{\lambda+2\mu}{\rho}}$ and the S-wave $v_s = \sqrt{\frac{\mu}{\rho}}$ are not equal. These two facts are enough to prove boundedness of the matrices. Applying the inverse Fourier transform and performing the change of variables $z = -\xi^2$, one has

$$w_2(0) = \left[R^s\int_{-\infty}^{0}\frac{dz}{\pi\sqrt{-z}(\Lambda_p-z)} + R^p\int_{-\infty}^{0}\frac{dz}{\pi\sqrt{-z}(\Lambda_s-z)}\right]w_1^0.$$

Let us draw attention to the equality

$$\int_{-\infty}^{0}\frac{dz}{\pi\sqrt{-z}(\Lambda-z)} = \frac{1}{\sqrt{\Lambda}} = f\big(\Lambda(\omega,\eta)\big)$$

for $\Lambda > 0$.The function $f(\Lambda)$ is the NtD map corresponding to the optimal PML for the scalar wave equation. Finally, the key equality is

$$w_2(0) = \big[R^s(\omega,\eta)f\big(\Lambda_s\big) + R^p(\omega,\eta)f\big(\Lambda_p\big)\big]w_1^0$$

which is equivalent to

$$\begin{bmatrix} u_x(0,\omega,\eta) \\ \sigma_{xy}(0,\omega,\eta) \end{bmatrix} = \big[R^s(\omega,\eta)f\big(\Lambda_s\big) + R^p(\omega,\eta)f\big(\Lambda_p\big)\big]\begin{bmatrix} u^0 \\ \sigma^0 \end{bmatrix}$$

up to a change of notation. □

2.3. Construction of finite-difference NtD map. In order to construct the finite-difference impedance, let us state the f-d NtD problem first. Introduce a staggered grid with two sets of points. The first one contains so-called "primary" points x_i, $i = 1,\dots,k+1$, where the vector w_2 is defined. The second set of points holds the "dual" ones $\hat{x}_i$, $i = 0,\dots,k$, where w_2 is stored. Let us assume, in addition, $x_1 = \hat{x}_0 = 0$ and define the steps by the rule $h_i = x_{i+1} - x_i$, $\hat{h}_i = \hat{x}_i - \hat{x}_{i-1}$, $i = 1,\dots,k$. In order to simplify the representation of

ETNA
Kent State University
http://etna.math.kent.edu

the finite-difference scheme, let us come back to the original notation of the variables, i.e., $w_1 = (\sigma_{xx}, u_y, \sigma_{yy})^T$, $w_2 = (u_x, \sigma_{xy})^T$, and $A^* w_1 = (\sigma_{xx}, u_y)^T$, so that the condition at the interface becomes $w_1^0 = (\sigma^0, u^0)^T$. We will use both notations to perform the construction of the f-d NtD map. In terms of the introduced grid, the finite-difference scheme for PML can be represented as

$$\begin{bmatrix} 0 & 0 & 0 & Y & 0 \\ 0 & 0 & 0 & 0 & Y \\ 0 & 0 & 0 & 0 & 0 \\ X & 0 & 0 & 0 & 0 \\ 0 & X & 0 & 0 & 0 \end{bmatrix} \begin{bmatrix} \vec{\sigma}_{xx} \\ \vec{u}_y \\ \vec{\sigma}_{yy} \\ \vec{u}_x \\ \vec{\sigma}_{xy} \end{bmatrix} + \begin{bmatrix} -a_1 I & 0 & -a_3 I & 0 & 0 \\ 0 & -\rho I & \theta I & 0 & 0 \\ -a_3 I & \theta I & -a_1 I & 0 & 0 \\ 0 & 0 & 0 & -\rho I & \theta I \\ 0 & 0 & 0 & \theta I & -a_2 I \end{bmatrix} \begin{bmatrix} \vec{\sigma}_{xx} \\ \vec{u}_y \\ \vec{\sigma}_{yy} \\ \vec{u}_y \\ \vec{\sigma}_{xy} \end{bmatrix} = \begin{bmatrix} 0 \\ 0 \\ 0 \\ \hat{h}_1^{-1} \mathbf{e}_1 \sigma^0 \\ \hat{h}_1^{-1} \mathbf{e}_1 u^0 \end{bmatrix}, \tag{2.7}$$

where the elements of the matrices are matrices themselves and their size is $k \times k$. The first component of the vector $\mathbf{e}_1$ is equal to one and all the rest are zeroes. The elements of the vectors are vector-columns with lengths equal to k. Matrices X and Y are

$$X = \begin{bmatrix} \hat{h}_1 & 0 & \dots & 0 \\ -\hat{h}_2 & \hat{h}_2 & & \vdots \\ 0 & \ddots & \ddots & 0 \\ & 0 & -\hat{h}_k & \hat{h}_k \end{bmatrix}, \qquad Y = \begin{bmatrix} -h_1 & h_1 & 0 & \\ 0 & \ddots & \ddots & 0 \\ \vdots & & -h_{k-1} & h_{k-1} \\ 0 & \dots & 0 & -h_k \end{bmatrix}.$$

The finite-difference solution at the interface $x = 0$ is $((u_x)_1, (\sigma_{xy})_1)^T = (w_2)_1$. Just as for the differential problem, the solution of the f-d can be constructed explicitly. Moreover, the following theorem holds.

THEOREM 2.2. *The solution of the problem (2.7) can be represented as*

$$\begin{bmatrix} (u_x)_1 \\ (\sigma_{xy})_1 \end{bmatrix} = \left[R^s(\omega, \eta) f^k(\Lambda_s) + R^p(\omega, \eta) f^k(\Lambda_p) \right] \begin{bmatrix} u^0 \\ \sigma^0 \end{bmatrix},$$

where matrices R^s and R^p coincide with the ones from Theorem 2.1, and functions $f^k(\lambda_j)$, $j = p, s$, are finite-difference NtD maps corresponding to the scalar wave equation with velocities v_j.

Proof. In order to solve the problem (2.7), it is convenient to symmetrize it. Let us introduce the matrix $A = C^{1/2} Y B^{-1/2} = -(B^{1/2} X C^{-1/2})^T$, where $B = \operatorname{diag}(\hat{h}_1, \dots, \hat{h}_k)$ and $C = \operatorname{diag}(h_1, \dots, h_k)$. Implementation of the diagonal transform $\operatorname{diag}(C^{1/2}, C^{1/2}, C^{1/2}, B^{1/2}, B^{1/2})$ allows one to obtain the system

$$\begin{bmatrix} -a_1 I & 0 & -a_3 I & A & 0 \\ 0 & -\rho I & \theta I & 0 & A \\ -a_3 I & \theta I & -a_1 I & 0 & 0 \\ -A^T & 0 & 0 & -\rho I & \theta I \\ 0 & -A^T & 0 & \theta I & -a_2 I \end{bmatrix} \begin{bmatrix} \breve{\sigma}_{xx} \\ \breve{u}_y \\ \breve{\sigma}_{yy} \\ \breve{u}_x \\ \breve{\sigma}_{xy} \end{bmatrix} = \begin{bmatrix} 0 \\ 0 \\ 0 \\ \sqrt{\hat{h}_1^{-1}} \mathbf{e}_1 \sigma^0 \\ \sqrt{\hat{h}_1^{-1}} \mathbf{e}_1 u^0 \end{bmatrix}.$$

ETNA
Kent State University
http://etna.math.kent.edu

With the help of the singular value decomposition of matrix A, one can simplify the system as follows:

$$\begin{bmatrix} -a_1 I & 0 & -a_3 I & D & 0 \\ 0 & -\rho I & \theta I & 0 & D \\ -a_3 I & \theta I & -a_1 I & 0 & 0 \\ -D & 0 & 0 & -\rho I & \theta I \\ 0 & -D & 0 & \theta I & -a_2 I \end{bmatrix} \begin{bmatrix} \bar{\sigma}_{xx} \\ \bar{u}_y \\ \bar{\sigma}_{yy} \\ \bar{u}_x \\ \bar{\sigma}_{xy} \end{bmatrix} = \begin{bmatrix} 0 \\ 0 \\ 0 \\ \sqrt{\hat{h}_1^{-1}}\mathbf{s}_1\sigma^0 \\ \sqrt{\hat{h}_1^{-1}}\mathbf{s}_1 u^0 \end{bmatrix},$$

where $\mathbf{s}_1$ is the vector consisting of the first components of the right singular vectors of the matrix A. One can see that the matrix of the system can be split into k independent matrices of the form

$$\begin{bmatrix} -a_1 & 0 & -a_3 & d_i & 0 \\ 0 & -\rho & \theta & 0 & d_i \\ -a_3 & \theta & -a_1 & 0 & 0 \\ -d_i & 0 & 0 & -\rho & \theta \\ 0 & -d_i & 0 & \theta & -a_2 \end{bmatrix} \begin{bmatrix} (\bar{\sigma}_{xx})_i \\ (\bar{u}_y)_i \\ (\bar{\sigma}_{yy})_i \\ (\bar{u}_x)_i \\ (\bar{\sigma}_{xy})_i \end{bmatrix} = \begin{bmatrix} 0 \\ 0 \\ 0 \\ \sqrt{\hat{h}_1^{-1}}s_{1i}\sigma^0 \\ \sqrt{\hat{h}_1^{-1}}s_{1i}u^0 \end{bmatrix}.$$

The system obtained is equivalent to (2.5) up to a change of variables, leaving $(\bar{u}_x)_i$ and $(\bar{\sigma}_{xy})_i$ the same. So we can write down the solution $((\bar{u}_x)_i, (\bar{\sigma}_{xy})_i)^T$ as

$$\begin{bmatrix} (\bar{u}_x)_i \\ (\bar{\sigma}_{xy})_i \end{bmatrix} = \left[R^s(\omega,\eta)\frac{\sqrt{\hat{h}_1^{-1}}s_{1i}}{d_i^2+\Lambda_s} + R^p(\omega,\eta)\frac{\sqrt{\hat{h}_1^{-1}}s_{1i}}{d_i^2+\Lambda_p} \right] \begin{bmatrix} u^0 \\ \sigma^0 \end{bmatrix}.$$

Due to the equivalence of the system considered and the system which appeared in the proof of Theorem 2.1, matrices R^s and R^p are given by the formulas (2.6). Performing the inverse transforms, one can derive the solution $(u_x)_1$ and $(\sigma_{xy})_1$ of the form

$$\begin{bmatrix} (u_x)_1 \\ (\sigma_{xy})_1 \end{bmatrix} = \left[R^s(\omega,\eta)\sum_{i=1}^{k}\frac{y_i}{\Lambda_s-\psi_i} + R^p(\omega,\eta)\sum_{i=1}^{k}\frac{y_i}{\Lambda_s-\psi_i} \right] \begin{bmatrix} u^0 \\ \sigma^0 \end{bmatrix},$$

where $y_i = s_{1i}^2/\hat{h}_1$ and $\psi_i = -d_i^2$. Let us now establish now the finite-difference NtD map

$$f^k(\Lambda) = \sum_{i=1}^{k}\frac{y_i}{\Lambda-\psi_i} = \frac{P^{k-1}(\Lambda)}{P^k(\Lambda)}.$$

Following [1], the rational function obtained coincides with the f-d NtD map for the PML for the scalar wave equation. □

Let us introduce a shorter notation for the f-d NtD map that will be useful for further investigations,

$$(w_2)_1 = \left[R^s(\omega,\eta)f^k(\Lambda_s) + R^p(\omega,\eta)f^k(\Lambda_p)\right] w_1^0.$$

2.4. Order of convergence. Let us define the discrepancy of the solution as

$$\delta = \|w_2(0) - (w_2)_1\| = \left\| \begin{bmatrix} u_x(0) \\ \sigma_{xy}(0) \end{bmatrix} - \begin{bmatrix} (u_x)_1 \\ (\sigma_{xy})_1 \end{bmatrix} \right\|.$$

ETNA
Kent State University
http://etna.math.kent.edu

We have the estimate,

$$\begin{aligned}\delta &= \left\| \left[f(\Lambda_s) - f^k(\Lambda_s)\right] R^s(\omega,\eta) w_1^0 + \left[f(\Lambda_p) - f^k(\Lambda_p)\right] R^p(\omega,\eta) w_1^0 \right\| \\ &\le \left\| f(\Lambda_s) - f^k(\Lambda_s) \right\| \left\| R^s w_1^0 \right\| + \left\| f(\Lambda_p) - f^k(\Lambda_p) \right\| \left\| R^p w_1^0 \right\|.\end{aligned}$$

Due to the boundedness of the matrices R^s and R^p and the input data, the terms $R^j w_1^0$ are bounded. So in order to investigate convergence, one should consider

$$\left\| f(\Lambda_j) - f^k(\Lambda_j) \right\| = \left\| \frac{1}{\sqrt{\Lambda_j}} - \sum_{i=1}^{k} \frac{y_i}{\Lambda_j - \psi_i} \right\|.$$

Following [1], let us use the norm of functions,

$$\left\| f(\Lambda_j) - f^k(\Lambda_j) \right\| = \max_{\Lambda \in [0,\Lambda_1]} \left| f(\Lambda_j) - f^k(\Lambda_j) \right|,$$

where Λ_1 is defined by the problem. As it was shown above, the functions $f(\Lambda_j)$, $j = p, s$, are the NtD maps of the scalar problem with velocities v_p and v_s, correspondingly. Let us consider the spectral parameters Λ_j in more detail. As soon as $\Lambda_j = v_j^{-2} - \theta^2$, it is easy to show that for propagative modes $\Lambda_j \in [0, v_j^{-2}]$. All isotropic elastic media satisfy the inequality $v_p > v_s$, so that

$$\Lambda_j \in \left[0, v_j^{-2}\right] \subseteq \left[0, v_s^{-2}\right].$$

We can also assume that $v_s = 1$. Otherwise, the problem can be remeasured to archive this property. Exploiting this embedding, we can derive the inequality

$$\begin{aligned}\left\| f(\Lambda_p) - f^k(\Lambda_p) \right\| &= \max_{\Lambda \in [0, v_p^{-2}]} \left| f(\Lambda) - f^k(\Lambda) \right| \\ &\le \max_{\Lambda \in [0,1]} \left| f(\Lambda) - f^k(\Lambda) \right| = \left\| f(\Lambda_s) - f^k(\Lambda_s) \right\|.\end{aligned}$$

Therefore, one can conclude that

$$\begin{aligned}\delta &\le \max_{\Lambda \in [0,1]} \left| f(\Lambda) - f^k(\Lambda) \right| \left(\left\| R^s(\omega,\eta) w_1^0 \right\| + \left\| R^p(\omega,\eta) w_1^0 \right\| \right) \\ &\le \max_{\Lambda \in [0,1]} \left| f(\Lambda) - f^k(\Lambda) \right| \left(\left\| R^s(\omega,\eta) \right\| + \left\| R^p(\omega,\eta) \right\| \right) \left\| \begin{bmatrix} u_y(0) \\ \sigma_{xx}(0) \end{bmatrix} \right\|.\end{aligned}$$

As was proven in [5], use of optimal rational approximation of the inverted square root allows one to satisfy estimate

$$\max_{\Lambda \in [0,1]} \left| \frac{1}{\sqrt{\Lambda}} - \sum_{i=1}^{k} \frac{y_i}{\Lambda - \psi_i} \right| \le C_1 e^{-\sqrt{k} C_2},$$

where C_1 and C_2 are constants given in [4]. Finally, one can derive the error estimate for optimal discretization of the PML for elasticity,

$$\delta \le C e^{-\sqrt{k} C_2},$$

where C is a bounded constant due to the limited nature of the Neumann data and the matrices R^s and R^p. Thus, implementation of optimal grids for the PML provides one with exponential order of convergence with respect to the number of grid points. For the artificial boundary conditions to be most effective, they need to be able to absorb not only the propagative modes of the solution, but also the evanescent ones. The proposed PML is optimal in terms of absorption of the propagative part. However, the evanescent part was left untreated. The obvious solution to this problem is to place these boundary conditions at a distance to receivers; this will ensure that the evanescent modes of the solution get absorbed.

ETNA
Kent State University
http://etna.math.kent.edu

2.5. Reconstruction of grid steps. The existence of the optimal discretization of PML for elasticity was proved above. This section presents the algorithm of the grid step computation when the rational approximation has been achieved already.

Suppose one already knows the rational function

$$f^k(\Lambda) = \sum_{i=1}^{k} \frac{y_i}{\Lambda - \psi_i},$$

where, following the proof of Theorem 2.2, parameters y_i are the first components of the right singular vectors of matrix A normalized over the first dual step. Variables ψ_i are equal minus squared singular values of the matrix. In order to recover the grid steps, one should reconstruct the matrix from the singular data. This problem can be reduced to the inverse spectral problem for symmetric tridiagonal matrices. It is easy to see that parameters y_i are normalized eigenvectors and ψ_i are eigenvalues of matrix $H = -A^T A$, which is tridiagonal and symmetric. The inverse spectral problem for these matrices is well studied; see, e.g., [3] for review.

Assume the matrix is already constructed. Let us write it down as

$$H = \begin{bmatrix} \alpha_1 & \beta_1 & 0 & \dots & 0 \\ \beta_1 & \alpha_2 & \beta_2 & & \vdots \\ 0 & \ddots & \ddots & \ddots & 0 \\ \vdots & & \beta_{k-2} & \alpha_{k-1} & \beta_{k-1} \\ 0 & \dots & 0 & \beta_{k-1} & \alpha_k \end{bmatrix},$$

where

$$\alpha_1 = \frac{1}{h_1 \hat{h}_1}, \qquad \beta_i = \frac{1}{h_i \sqrt{\hat{h}_i \hat{h}_{i+1}}}, \qquad i = 1, \dots, k-1,$$

$$\alpha_i = \frac{1}{\hat{h}_i} \left(\frac{1}{h_i} + \frac{1}{h_{i-1}} \right), \qquad i = 2, \dots, k.$$

In order to recover the grid, steps one should invert these formulas and the initial condition

$$\sum_{i=1}^{k} y_i = \sum_{i=1}^{k} \frac{s_{1i}^2}{\hat{h}_1} = \frac{1}{\hat{h}_1}.$$

Finally, one gets the recursive algorithm to construct the steps

$$\hat{h}_1 = \frac{1}{\sum_{i=1}^{k} y_i}, \qquad \hat{h}_i = \frac{1}{\beta_{i-1}^2 h_{i-1}^2 \hat{h}_{i-1}}, \qquad i = 2, \dots, k,$$

$$h_1 = -\frac{1}{\hat{h}_1 \alpha_1}, \qquad h_i = -\frac{1}{\alpha_i \hat{h}_i + 1/h_{i-1}}, \qquad i = 2, \dots, k.$$

The properties of the algorithm are discussed in [4]. The examples of the grid steps for spectral interval $\Lambda \in [0, 1]$ for different numbers of the points inside the PML are (provided by

ETNA
Kent State University
http://etna.math.kent.edu

L. Knizhnerman)

$$
\begin{aligned}
&k = 2\\
&h_1 = 2.365487995263112, && \hat{h}_1 = 6.180339887498947\cdot 10^{-1},\\
&h_2 = 52.467327734734150, && \hat{h}_2 = 7.486067977499783,\\
&k = 3\\
&h_1 = 1.653239359561106, && \hat{h}_1 = 4.808627161472366\cdot 10^{-1},\\
&h_2 = 9.382459638953518, && \hat{h}_2 = 3.780563735130913,\\
&h_3 = 222.6171432329176, && \hat{h}_3 = 30.5232141352186,\\
&k = 5\\
&h_1 = 1.148373258296764, && \hat{h}_1 = 3.56609347906754\cdot 10^{-1},\\
&h_2 = 4.019019551581278, && \hat{h}_2 = 2.229274743906089,\\
&h_3 = 15.11442138770956, && \hat{h}_3 = 7.492603535587417,\\
&h_4 = 88.28452858074355, && \hat{h}_4 = 33.90525047350573,\\
&h_5 = 2167.441887240847, && \hat{h}_5 = 295.080551875105.
\end{aligned}
$$

3. Finite-difference schemes. First of all let us recall the Virieux finite-difference scheme [9] on staggered grids for isotropic elasticity. We drop the "hat" over variables inthe time domain because we will no longer consider any equations or functions inthe spectral domain. In order to simplify the representation of the f-d scheme, let us introduce the operators

$$
\begin{aligned}
D_{ij}^{q-1/2} f &= \frac{f_{ij}^{q} - f_{ij}^{q-1}}{\tau}, & D_{ij}^{q} f &= \frac{f_{ij}^{q+1/2} - f_{ij}^{q-1/2}}{\tau},\\
\big(L^x\big)_{ij}^{q} f &= \frac{f_{ij}^{q} - f_{i-1j}^{q}}{h_{i-1}}, & \big(\hat{L}^x\big)_{ij}^{q} f &= \frac{f_{i+1j}^{q} - f_{ij}^{q}}{\hat{h}_i},\\
\big(L^y\big)_{ij}^{q} f &= \frac{f_{ij}^{q} - f_{ij-1}^{q}}{H_{j-1}}, & \big(\hat{L}^y\big)_{ij}^{q} f &= \frac{f_{ij+1}^{q} - f_{ij}^{q}}{\hat{H}_j},
\end{aligned}
$$

where $h_i = x_{i+1} - x_i$, $\hat{h}_i = \hat{x}_{i+1} - \hat{x}_i$, and the same for the second spatial direction. This notation differs from the notation used for the grid construction, but is more natural for the representation of the finite-difference scheme. The Virieux scheme [9] is

$$
\begin{aligned}
\rho D_{ij}^{q-1/2}(u_x) &= \big(L^x\big)_{ij}^{q-1/2}(\sigma_{xx}) + \big(\hat{L}^y\big)_{ij}^{q-1/2}(\sigma_{xy}),\\
\rho D_{ij}^{q-1/2}(u_y) &= \big(\hat{L}^x\big)_{ij}^{q-1/2}(\sigma_{xy}) + \big(L^y\big)_{ij}^{q-1/2}(\sigma_{yy}),\\
D_{ij}^{q}(\sigma_{xx}) &= (\lambda+2\mu)\big(\hat{L}^x\big)_{ij}^{q}(u_x) + \lambda\big(\hat{L}^y\big)_{ij}^{q}(u_y),\\
D_{ij}^{q}(\sigma_{yy}) &= \lambda\big(\hat{L}^x\big)_{ij}^{q}(u_x) + (\lambda+2\mu)\big(\hat{L}^y\big)_{ij}^{q}(u_y),\\
D_{ij}^{q}(\sigma_{xy}) &= \mu\big(L^x\big)_{ij}^{q}(u_y) + \mu\big(L^y\big)_{ij}^{q}(u_x).
\end{aligned}
\tag{3.1}
$$

Superscripts denote the number of the time instants. Subscripts denote the numbers of points in x and y directions, correspondingly. So $f_{ij}^{n} = f(t^q, x_i, y_j)$. If equidistant grids are

ETNA
Kent State University
http://etna.math.kent.edu

used, then $h_i = \hat{h}_i = h_x$, $H_j = \hat{H}_j = h_y$, and $f_{ij}^n = f(\tau n, ih_x, jh_y)$. The scheme is explicit, conditionally stable, and provides one with the second order of approximation [9]. As soon as wave processes are simulated, the dispersion properties of the scheme should be taken into account. This means that the velocity of the finite-difference solution depends on the discretization and converges to the true solution when the grid is refined. The difference between the velocities is crucial for later discussion of the reflection coefficients at the interface between the target area and the PML.

3.1. Finite-difference scheme for PML. The pure imaginary change of variables performed in spectral domain to construct the optimal PML leads one to the change in time domain,

$$\frac{\partial}{\partial x} \to \frac{\partial^2}{\partial x \partial t}.$$

Using this substitution and the matching conditions,

$$\begin{aligned} \big[u_x\big]|_{x=0} &= 0, \qquad \big[u_y\big]|_{x=0} = 0, \\ \big[\sigma_{xx}\big]|_{x=0} &= 0, \qquad \big[\sigma_{xy}\big]|_{x=0} = 0, \end{aligned}$$

one can construct the finite-difference scheme for the PML. In the present notation, $[f]|_{x=0} = f(0+) - f(0-)$ means the jumps of the function. Due to the change of variables presented above, functions u_x, σ_{xx}, and σ_{yy} should be defined at the integer knots while all others are defined at fractional ones. Thus, the finite-difference scheme for the PML becomes implicit. The advantage of the scheme is the possibility of splitting it into two independent ones. The first scheme is used to compute the solution at integer time layers. The second one allows the update of the solution at fractional instants.

Opposite to the notation used for the construction of the optimal discretization, it is convenient to introduce the grid nodes by the following rule. Let both "primary" and "dual" points x_i and $\hat{x}_i$ be correspondingly defined for $i = 0, \ldots, k$. Moreover, due to the construction of the optimal grids, let us require $x_0 = \hat{x}_0 = 0$. Therefore, the negative indexes correspond to the target area where the Virieux scheme is used and the positive ones including zero represent the PML. The finite-difference scheme inside the PML is

$$\begin{aligned} \rho D_{ij}^{q-1/2}(u_x) &= \big(\hat{L}^x\big)_{ij}^{q-1/2} D_{ij}^{q-1/2}\big(\sigma_{xx}\big) \\ &\quad + \big(\hat{L}^y\big)_{ij}^{q-1/2}\big(\sigma_{xy}\big), \quad i = 0, \ldots, k-1, \\ \big(u_x\big)_{kj}^{q} &= 0, \\ D_{ij}^{q-1/2}\big(\sigma_{xx}\big) &= (\lambda + 2\mu)\big(L^x\big)_{ij}^{q-1/2} D_{ij}^{q-1/2}\big(u_x\big) \\ &\quad + \lambda\big(\hat{L}^y\big)_{ij}^{q-1/2}\big(u_y\big), \quad i = 1, \ldots, k, \\ \frac{\rho h_x}{\tau} D_{0j}^{q-1/2}\big(u_x\big) &= D_{0j}^{q-1/2}\big(\sigma_{xx}\big) + \frac{\big(\sigma_{xx}\big)_{0j}^{q-1} - \big(\sigma_{xx}\big)_{-1j}^{q-1/2}}{\tau/2} \\ &\quad + \frac{h_x}{\tau}\big(\hat{L}^y\big)_{0j}^{q-1/2}\big(\sigma_{xy}\big), \\ D_{ij}^{q-1/2}\big(\sigma_{yy}\big) &= \lambda\big(L^x\big)_{ij}^{q-1/2} D_{ij}^{q-1/2}\big(u_x\big) \\ &\quad + (\lambda + 2\mu)\big(\hat{L}^y\big)_{ij}^{q-1/2}\big(u_y\big), \quad i = 1, \ldots, k, \end{aligned} \tag{3.2}$$

ETNA
Kent State University
http://etna.math.kent.edu

$$
\begin{aligned}
D^q_{ij}(\sigma_{xy}) &= \mu\big(\hat{L}^x\big)^q_{ij} D^q_{ij}(u_y) \\
&\quad + \mu\big(L^y\big)^q_{ij}(u_x), \quad i = 0, \dots, k-1, \\
\big(\sigma_{xy}\big)^{q+1/2}_{kj} &= 0, \\
\rho D^q_{ij}(u_y) &= \big(L^x\big)^q_{ij} D^q_{ij}(\sigma_{xy}) \\
&\quad + \big(\hat{L}^y\big)^q_{ij}(\sigma_{yy}), \quad i = 1, \dots, k, \\
\frac{h_x}{\mu\tau} D^q_{0j}(\sigma_{xy}) &= D^q_{0j}(u_y) + \frac{\big(u_y\big)^{q-1/2}_{0j} - \big(u_y\big)^q_{-1j}}{\tau/2} \\
&\quad + \frac{h_x}{\tau}\big(L^y\big)^q_{0j}(u_x).
\end{aligned} \tag{3.3}
$$

The first system is used to update the solution at the integer time layers, and the second one allows computation of the solution at fractional instants. In order to deal with the implicit finite-difference scheme, the properties of the matrices should be investigated in detail. The first of them is the singularity of the matrices. The second one is the condition number. It is possible to prove the nonsingularity analytically, but the conditioning can only be investigated numerically.

3.2. Properties of the matrices.

3.2.1. Nonsingularity. One can see that the systems (3.2) and (3.3) excluding the equations for the σ_{yy} coincide up to coefficients. The nonsingularity of the matrix can be shown for the matrix of the (3.3), and the result will hold for the other system.

Let us rewrite the system (3.3) as $Mx = b$, where

$$x = (D^q_{0j}(\sigma_{xy}), \dots, D^q_{k-1j}(\sigma_{xy}), D^q_{0j}(u_y), \dots, D^q_{kj}(u_y))^T,$$

and M is

$$M = \begin{bmatrix} I_k & B \\ F & I_{k+1} \end{bmatrix}.$$

Matrices I_k are $k \times k$ unitary ones,

$$B = \begin{bmatrix} \beta_1 & -\beta_1 & & 0 \\ & \ddots & \ddots & \\ 0 & & \beta_k & -\beta_k \end{bmatrix}, \qquad F = \begin{bmatrix} -\alpha_0 & 0 & \dots & 0 \\ \alpha_1 & -\alpha_1 & & \vdots \\ 0 & \ddots & \ddots & 0 \\ \vdots & & \alpha_{k-1} & -\alpha_{k-1} \\ 0 & \dots & 0 & \alpha_k \end{bmatrix}.$$

All the elements of the matrices are greater than zero, $\alpha_0 = h_x/(\tau\mu) > 0$, $\alpha_i = 1/(h_i\rho) > 0$, and $\beta_i = \mu/\hat{h}_i > 0$ for $i = 1, \dots, k$.

Let us introduce two sets of matrices. The first one is

$$D_i = \begin{bmatrix} I_{k-i+1} & B_i \\ F_i & I_{k-i+1} \end{bmatrix},$$

ETNA
Kent State University
http://etna.math.kent.edu

where I_n is the unitary matrix of the size n. The other is

$$F_i = \begin{bmatrix} \alpha_i & -\alpha_i & & 0 \\ 0 & \ddots & \ddots & \\ \vdots & & \alpha_{k-1} & -\alpha_{k-1} \\ 0 & \dots & 0 & \alpha_k \end{bmatrix}, \qquad B_i = \begin{bmatrix} -\beta_i & 0 & \dots & 0 \\ \beta_{i+1} & -\beta_{i+1} & & \vdots \\ & \ddots & \ddots & 0 \\ 0 & & \beta_k & -\beta_k \end{bmatrix}.$$

The second set consists of matrices

$$\tilde{D}_i = \begin{bmatrix} I_{k-i} & \tilde{B}_i \\ \tilde{F}_i & I_{k-i+1} \end{bmatrix},$$

where $\tilde{F}_i$ and $\tilde{B}_i$ are obtained from F and B correspondingly by annihilating first the i rows and columns. It is easy to see that the following recurrence relations and initial conditions hold,

$$\begin{aligned} \det\left(D_i\right) &= \det\left(\tilde{D}_i\right) + \alpha_i\beta_i \det\left(D_{i+1}\right), \\ \det\left(\tilde{D}_i\right) &= \det\left(D_{i+1}\right) + \alpha_i\beta_{i+1} \det\left(\tilde{D}_{i+1}\right), \end{aligned}$$

$$\begin{aligned} \det\left(D_k\right) &= 1 + \alpha_k\beta_k, \\ \det\left(\tilde{D}_k\right) &= 1. \end{aligned}$$

Taking into account positivity of the properties α_i and β_i, one can prove that determinants $\det(D_1)$ and $\det(\tilde{D}_1)$ are strictly positive for any k by using mathematical induction.

It is clear that the determinant of the matrix M can be represented, by annihilating the $(k+1)$st column, as

$$\det(M) = -\det(D_1) - \beta_1 \det(\tilde{D}_1).$$

If $\beta_1 > 0$, $\det(D_1) > 0$, and $\det(\tilde{D}_1) > 0$, then one can conclude that $\det(M) < 0$ for any medium parameters and grid steps. Therefore, the matrix is not singular for any appropriate media parameters and grid steps.

All the same argument can be used for the matrix of the system (3.2).

3.2.2. Conditioning. Due to the high complexity of the analytical investigations, the conditioning is studied numerically. On the one hand, if one deals with nondimensional variables and media parameters, i.e., the velocities and the density are about 10^0, then the condition numbers of the matrices (3.2) and (3.3) are between 10^0 and 10^1. On the other hand, if dimensional variables are used, then the velocities and the density are about 10^3. This leads one to Lame parameters λ and μ equal to $10^8 - 10^{10}$, so the condition numbers of the matrices rise up to $10^{12} - 10^{16}$. It is clear that the matrices become hard to invert properly and preconditioning is required.

The preconditioning of this matrix can be done explicitly without additional cost. Let us consider the system (3.3) written in the form

$$\begin{bmatrix} I_k & B \\ F & I_{k+1} \end{bmatrix} \begin{bmatrix} D^q_{*j}(\sigma_{xy}) \\ D^q_{*j}(u_y) \end{bmatrix} = \begin{bmatrix} f_1 \\ f_2 \end{bmatrix},$$

ETNA
Kent State University
http://etna.math.kent.edu

where vectors

$$D^q_{*j}(\sigma_{xy}) = \left(D^q_{0j}(\sigma_{xy}), \ldots, D^q_{k-1j}(\sigma_{xy})\right)^T,$$
$$D^q_{*j}(u_y) = \left(D^q_{0j}(u_y), \ldots, D^q_{kj}(u_y)\right)^T,$$

and the right-hand sides f_1 and f_2 are defined by the system. Their exact representation is not required for subsequent considerations, so we omit it. The matrices F and B were introduced in the previous section. Let us consider the linear transform

$$\begin{bmatrix} \frac{1}{\sqrt{v_s}} I_k & 0 \\ 0 & \sqrt{v_s} I_{k+1} \end{bmatrix} \begin{bmatrix} I_k & B \\ F & I_{k+1} \end{bmatrix} \begin{bmatrix} \sqrt{v_s} I_k & 0 \\ 0 & \frac{1}{\rho\sqrt{v_s}} I_{k+1} \end{bmatrix} = \begin{bmatrix} I_k & \tilde{B} \\ \tilde{F} & I_{k+1} \end{bmatrix}.$$

The matrices $\tilde{B}$ and $\tilde{F}$ are

$$\tilde{B} = \begin{bmatrix} \tilde{\beta}_1 & -\tilde{\beta}_1 & & 0 \\ & \ddots & \ddots & \\ 0 & & \tilde{\beta}_k & -\tilde{\beta}_k \end{bmatrix}, \qquad \tilde{F} = \begin{bmatrix} -\tilde{\alpha}_0 & 0 & \cdots & 0 \\ \tilde{\alpha}_1 & -\tilde{\alpha}_1 & & \vdots \\ 0 & \ddots & \ddots & 0 \\ \vdots & & \tilde{\alpha}_{k-1} & -\tilde{\alpha}_{k-1} \\ 0 & \cdots & 0 & \tilde{\alpha}_k \end{bmatrix},$$

where $\alpha_0 = h_x/(\tau v_s)$, $\alpha_i = v_s/h_i$, and $\beta_i = v_s/\hat{h}_i$, $i = 1, \ldots, k$. Let us rcall that the construction of the optimal grid was performed for the dimensionless problem, i.e., $v_s = 1$. Denote h^0_i as the steps corresponding to this problem. In order to use the grid for the problem with physical parameters, the steps should be stretched as $h_i = v_s h^0_i$. The statements presented allow one to conclude that the preconditioning described above maps the matrix to the one corresponding to the dimensionless problem. Consequently, the condition number of a new matrix is about $10^0 - 10^1$ and this matrix can be inverted easily.

A slightly modified procedure can be applied to the system (3.2) after changing v_s to v_p. In this case, the steps of the optimal discretization presented above should be multiplied by the factor $v_p/v_s \approx \sqrt{3}$. Because the ratio is about 10^0, this does not have a strong effect on the condition number of the matrix.

Taking everything into account, one can compute the optimal discretization of the PML for the dimensionless problem. With the help of the given steps, one is able to construct the matrices (3.2) and (3.3) without coming back to the physical scale. One should also mention that computations of the square roots of the velocities can be avoided, so this preconditioning does not increase complexity of the problem.

4. Numerical experiments. In order to illustrate the approach, two types of the numerical experiments were performed.

The first experiment was done to investigate the reflection coefficients connected with the interface between the target area and the PML. Due to the difference between the f-d velocity and the velocity introduced by differential statement, these coefficients depend on discretizations of both the PML and the target area. The numerical investigation of the reflections was performed for homogenous media. The computational domain was 3000 meters in the horizontal direction and 1500 meters in the vertical direction. The source was placed at a distance of two wavelengths from both the lower and the right boundaries. The signal was recorded along the horizontal line at a depth of 750 meters. This geometry allowed us to deal with the reflections from the bottom boundary for a wide range of incident angles from

ETNA
Kent State University
http://etna.math.kent.edu

0 to $5\pi/12$. The parameters of the medium were: $v_p = 4000\,m/s$, $v_s = 2300\,m/s$, and the density $\rho = 2500kg/m^3$. The Ricker pulse with dominant frequency of 30 Hz was used as a source function. As soon as it is possible to emit P- and S-waves separately in the isotropic medium, the experiments were performed for each wave independently. The discretizations of the regular domain were 20, 35, and 70 points per wavelength (ppw). The Courant stability ratio was 0.7. The number of points inside the PML varied from 3 to 15. Figures 4.1–4.3 represent the averaged reflection coefficients in percent for over all incident angles, i.e., for angles between 0 and $5\pi/12$. One can see the exponential decay of the reflections when the width of the PML increases. Nevertheless, the reflection coefficients converge to some nonzero limit. This limit is due to difference between the true velocity which was used to construct the PML discretization and the f-d velocity in the propagative part, and decreases from 0.5% to 0.05% as we refine the grid from 20 ppw to 75 ppw.

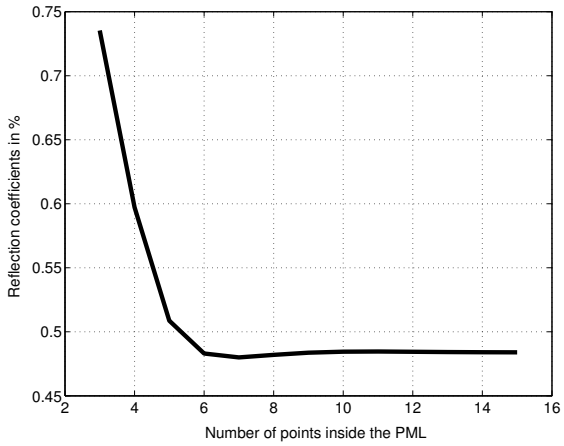

FIG. 4.1. *Averaged reflection coefficients in percent as a function of PML's depth measured in points. The grid inside the target area has 20 ppw.*

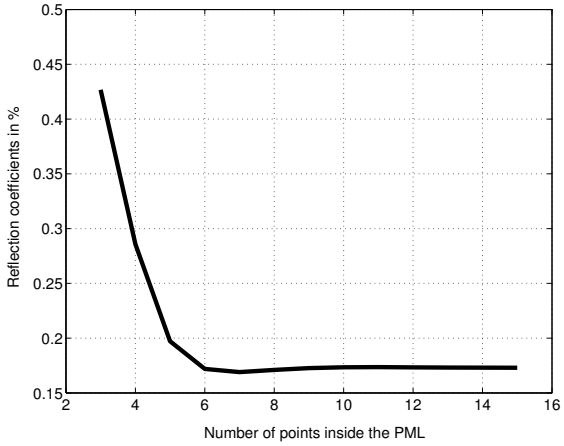

FIG. 4.2. *Averaged reflection coefficients in percent as a function of PML's depth measured in points. The grid inside the target area has 35 ppw.*

A similar experiment was performed for the surface wave which appears if the source is situated close enough to the free surface. The series of experiments was done for the source

ETNA
Kent State University
http://etna.math.kent.edu

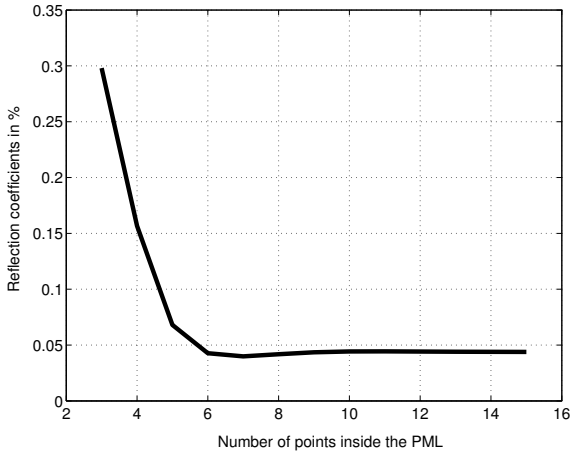

FIG. 4.3. *Averaged reflection coefficients in percent as a function of PML's depth measured in points. The grid inside the target area has 70 ppw.*

located at the depth of one tenth of dominant wavelength. Such geometry guarantees the existence of a strong surface wave. The incident angle for this wave is about zero, so only the discretizations of both PML and target area varied. The result for this wave coincided with the ones presented for the P- and S-waves. A Rayleigh wave usually has high amplitude and short wavelength. Hence, its reflections from the PML, according to the experiments performed, can be even stronger than the efficient signal propagated inside the target area. This shows the restriction of the present approach. In order to perform a simulation with near-surface sources, a fine grid with more than 70 ppw for the surface wave should be used in horizontal direction at least in vicinity of the PML's interface.

It is known that the classical PML is stable for isotropic acoustic problem; however, mild instability may occur in some layered elastic media. At the same time, analytical investigation of the PML's stability is an individual and nontrivial problem. So here we will not attempt it and will restrict ourselves to the numerical experiments only. The second type of experiment was performed for numerical investigation of the PML's stability. The first set of experiments was performed for homogenous media. The target area used for these experiments was 1000 meters over 1000 meters. The elastic velocities were $v_p = 4000$ meters per second, $v_s = 2300$ m/s, and the density $\rho = 2500\,\mathrm{kg/m^3}$. The Ricker pulse with dominant frequency 30 Hz was used as a source. It was located exactly at the center of the domain. The equidistant discretization of the target area with 20 ppw for the S-wave was performed. This grid provided about 35 ppw for the P-wave. The Courant stability ratio was 1 for the P-wave. The PML was introduced at all the boundaries except one where the free-surface boundary conditions were exploited. The elastic energy inside the domain was registered at all instants when the source had already stopped radiating. The energy level would not have changed if no PML had been used. In presence of PML, the energy decayed each time when a wave came into the PML. This effect can be observed in Figure 4.4, which represents the change of energy or energy profile depending on the time of computation. When the instability was taking place, the energy began growing exponentially; see Figure 4.4. The figure represents the energy profile for PML with 3 points. The experiment was performed for a long enough time for the instability effect to be seen. Figure 4.5 represents the times when the energy achieves its minimum. After this moment, the effect of instability begins to play the principal role on the results. One can see that the time when instability appears increases exponentially with respect to the number of points used inside the PML.

ETNA
Kent State University
http://etna.math.kent.edu

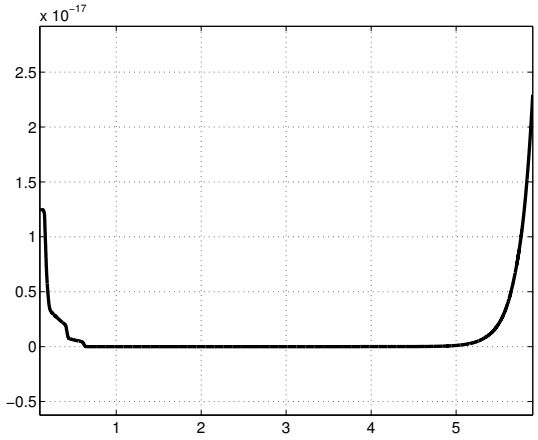

FIG. 4.4. *Total elastic energy inside the target area as a function of time. PML has 3 points. Horizontal axis represents time in seconds, vertical one denotes the energy level.*

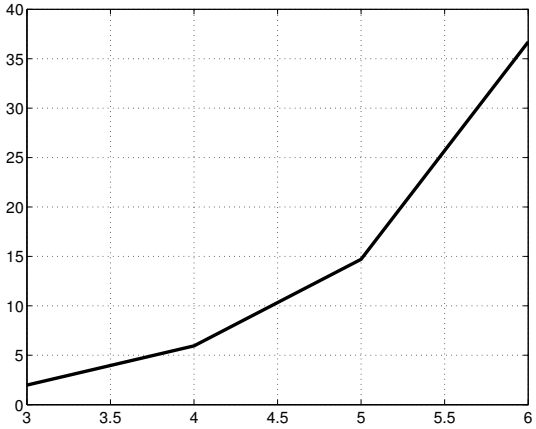

FIG. 4.5. *Time when the energy achieved its minimum (vertical axis) as a function of the number of grid points inside the PML (horizontal axis). Experiment was performed for homogenous media.*

The second set of experiments for numerical investigation of the PML's stability was performed for layered media. The model is represented in Figure 4.6. It consisted of three thick layers with the same depth of about 333 meters whose properties vary strongly. The media parameters inside the top one were $v_p = 2000$ m/s, $v_s = 1300$ m/s, and $\rho = 2000\,\text{kg/m}^3$; the parameters in the middle one were $v_p = 4000$ m/s, $v_s = 2300$ m/s, and $\rho = 2500\,\text{kg/m}^3$, and the bottom one had $v_p = 3200$ m/s, $v_s = 2000$ m/s, and $\rho = 3000\,\text{kg/m}^3$. The Ricker pulse with dominant frequency 30 Hz was used as a source and it was placed at point $(500, 100)$. One can see that the thicknesses of the layers were much higher than the minimal wavelength. Figure 4.7 represents the time when energy achieved its minimum with respect to the number of points inside the PML. These experiments show appropriate coincidence of the time when instability appears with the one for homogenous media. The difference of time scales in Figures 4.5 and 4.7 appears due to the different number of grid points used in the two experiments and rapid exponential growth of the functions. It should be mentioned that realistic geophysical experiments are not performed for such long times, so the proposed PML's construction can be considered stable for appropriate times.

ETNA
Kent State University
http://etna.math.kent.edu

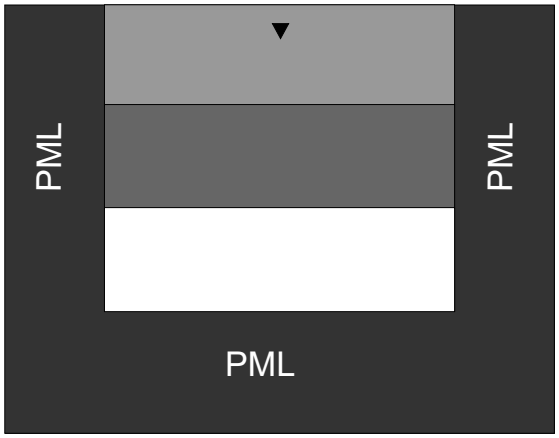

FIG. 4.6. *The model for the layered media experiment.*

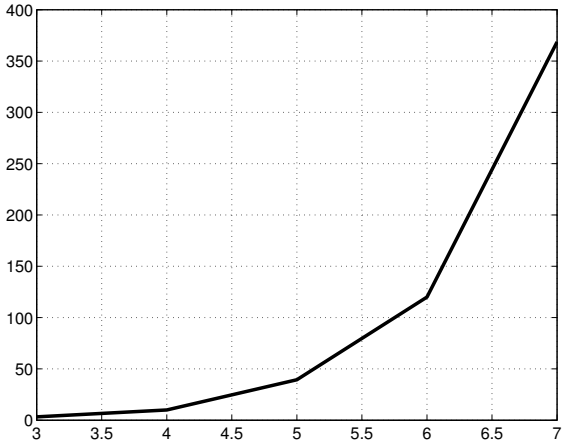

FIG. 4.7. *Time when the energy achieved its minimum (vertical axis) as a function of the number of grid points inside the PML (horizontal axis). Experiment was performed for layered media containing three thick layers.*

5. Conclusions. The optimal grid approach is extended to the elasticity problem. Optimal PML is developed for homogenous media and supported with all necessary proofs. This PML allows one to reach suitable reduction of the reflections for all incident angles. In the presence of no surface wave, the approach can be efficiently used for domain truncation problems for elasticity. In case of a near-surface source, optimal PML can be used together with grid refinement techniques in the vicinity of the interface to get rid of the surface wave. This approach makes it possible to totally decrease the computational time because the high precision of the solution can be reached using a small number of grid points.

According to the experiments presented, the time when instability exerts a strong influence on the solution depends on the number of grid points inside the PML zone. Moreover, this time increases exponentially as a function of thickness of the PML's discretization. In spite of the fact that the experiments presented demonstrate appropriate convergence and stability properties of the PML for layered media, they do not prove its stability for arbitrary inhomogenous media. Therefore, all necessary theoretical investigations of the optimal PML stability should be done.

ETNA
Kent State University
http://etna.math.kent.edu

REFERENCES

[1] S. ASVADUROV, V. DRUSKIN, M. GUDDATI, AND L. KNIZHNERMAN, *On optimal finite-difference approximation of pml*, SIAM J. Numer. Anal., 41 (2003), pp. 287–305.

[2] J.-P. BERENGER, *A perfectly matched layer for the absorption of electromagnetic waves*, J. Comput. Phys., 114 (1994), pp. 185–200.

[3] D. BOLEY AND G. H. GOLUB, *A survey of matrix inverse eigenvalue problems*, Inverse Problems, 3 (1987), pp. 595–622.

[4] V. DRUSKIN AND L. KNIZHNERMANN, *Gaussian spectral rules for the three-point second differences: I. a two-point positive definite problem in a semi-infinite domain*, SIAM J. Numer. Anal., 37 (1999), pp. 403–422.

[5] ———, *Gaussian spectral rules for second order finite-difference schemes*, Numer. Algorithms, 25 (2000), pp. 139–159.

[6] B. ENGQUIST AND A. MAJDA, *Absorbing boundary conditions for the numerical simulation of waves*, Math. Comp., 31 (1977), pp. 629–651.

[7] M. GUDDATI AND J. TASSOULAS, *Accurate radiation boundary conditions for the linearized euler equations in cartesian domains*, J. Comput. Acoust., 8 (1998), pp. 139–156.

[8] T. HAGSTROM AND J. GOODRICH, *Accurate radiation boundary conditions for the linearized euler equations in cartesian domains*, SIAM J. Sci. Comput., 24 (2003), pp. 770–795.

[9] J. VIRIEUX, *P-sv wave propagation in heterogeneous media: Velocity-stress finite-difference method*, Geophysics, 51 (1986), pp. 889–901.